



## Research articles

### UV-assisted direct write of polymer-bonded magnets

Alan Shen <sup>a</sup>, Callum P. Bailey <sup>b</sup>, Anson W.K. Ma <sup>a</sup>, Sameh Dardona <sup>b,\*</sup>



<sup>a</sup> Department of Chemical and Biomolecular Engineering & Institute of Materials Science, University of Connecticut, Storrs, CT 06269, USA

<sup>b</sup> Physical Sciences Department, United Technologies Research Center, East Hartford, CT 06118, USA

#### ARTICLE INFO

##### Article history:

Received 11 January 2018

Accepted 31 March 2018

Available online 13 April 2018

#### ABSTRACT

This work presents a novel fabrication technique called “UV-assisted Direct Write (UADW)”, which combines extrusion-based direct write (DW) and *in situ* layer-by-layer UV curing to fabricate polymer-bonded permanent magnets of arbitrary shapes at room temperature. The process requires minimal post heat treatment and therefore preserves the magnetic properties of the raw powder in the printed product. Experimentation achieved a maximum solid loading of printable ink of 60% by volume, or 91% by weight. Samples with 60 vol.% nominal particle concentration exhibited remanence of 3.80 kG (52% of raw powder value) and intrinsic coercivity of 9.50 kOe. Magnetized samples showed no reduction in intrinsic coercivity, which proves good curing of the final product and good bonding between particles and binder. Compared to other 3D-printed magnets reported in the literature, UADW magnets possess the highest intrinsic coercivity with one of the highest magnetic remanence values.

© 2018 Elsevier B.V. All rights reserved.

## 1. Introduction

Magnets have a wide range of industrial and commercial applications. Magnets enable physical tasks by attracting or repelling ferric materials and perform a variety of electrical tasks: e.g., creating an electric current in a generator or alternator, or enhancing performance of electromagnetic devices such as inductors [1]. Additionally, magnets and magnetic patterns facilitate high resolution sensing such as tracking the speed or the position of a moving piston or a rotating shaft. However, the creation of magnets with the unique shapes and field patterns needed to perform these functions generally entails subtractive machining of a larger permanent magnet, resulting in material waste and limiting the design space. The design freedom of additive manufacturing (AM), or 3D printing, has recently inspired research into novel techniques for magnet manufacturing. While AM polymer-bonded magnets exhibit a lower maximum energy product ( $BH_{max}$ ) than their sintered counterparts, the fabrication of polymer-bonded magnets offers a number of advantages over conventional processes. High-temperature sintering is not required, so magnet fabrication can integrate low-temperature technologies such as digital light processing (DLP), conductive ink deposition [2], and pick-and-place [3] to create multifunctional components *in situ*. No molds are required, reducing tooling costs and manufacturing time. Printed bonded

magnets allow increased design freedom with the ability to create complex internal geometries. These designs can be tweaked, printed, and iterated rapidly, facilitating the design process and reducing cost. Printed magnets can either be coated [4] onto or embedded [5] within other materials to build microrobots or sensors with minimal material waste.

Several recent studies contribute to the state-of-the-art for 3D printing of magnets. Huber et al. [6] printed nylon-bonded rare-earth magnets through fused deposition modeling (FDM) and compared their performance with magnets fabricated by injection molding. Printed magnets had a density of 3.6 g/cm<sup>3</sup>, lower than the 4.35 g/cm<sup>3</sup> density achieved by injection molding [6], indicating FDM printed magnets exhibit higher process-induced porosity and thus weaker magnetic properties [7]. Paranthaman et al. [8] report a specialized FDM technique for printed magnets, coined Big Area Additive Manufacturing (BAAM), capable of matching the magnetic properties of injection-molded magnets. Paranthaman et al. [9] also fabricated magnets with binder jetting and achieved 46 vol.% density of Neodymium Iron Boron (NdFeB) raw powder. Compton et al. [10] report extrusion-based direct write of 36.5 vol.% magnetic material parts with post heat curing.

Current AM technologies have unlocked considerable design freedom but still face shortcomings in fabrication of magnets [11]. Typically, AM fabrication methodologies require a relatively aggressive post heat treatment process (>100 °C) after completion of the printing process, which can cause non-uniform heating of the component and structural deformation. Evaporation of solvent and binders can increase the porosity of the printed magnet and

\* Corresponding author at: United Technologies Research Center, 411 Silver Ln, East Hartford, CT 06118, USA.

E-mail address: [dardona@utrc.utc.com](mailto:dardona@utrc.utc.com) (S. Dardona).

yield a rough surface, rendering such methods inappropriate for printing of fine magnetic patterns. Often a post encapsulation of polyurethane is needed to reduce surface roughness [8]. Furthermore, while increasing magnetic particle loading increases the energy product of printed magnets, both FDM and BAAM processes report a drop in the intrinsic coercivity of printed samples compared with the coercivity of the raw material powder, probably due to the high temperature extrusion (300 °C) of the filament material during printing. To fully realize the advantages of AM technology for printing magnets and to ensure repeatability, we must understand the effects of ink properties and printing parameters on subsequent mechanical and magnetic properties.

A common 3D printing technology, stereolithography (SLA) is widely used for medical modeling and industrial prototyping and utilizes photopolymerization to build three-dimensional solid objects [12]. Most commercial SLA machines can only print with a limited choice of photopolymer resins and preprogrammed printing parameters, restricting the versatility of this technology [13]. In addition, the post processing time for resin removal is lengthy and material waste is often inevitable. To date, the relevant literature features no reports on SLA-printed magnets.

Direct write (DW) is an AM technique enabling the direct deposition of functional or structural patterns using various materials, without utilizing photo-masks or stencils [14]. The technique employs an ink-deposition nozzle to create 2D or 3D material patterns with desired architecture and composition on a computer-controlled translation stage [15]. Extrusion-based DW typically utilizes nano- or micro-particle suspensions to provide intricate details and a smooth surface finish [16]. Tuning the rheological properties of DW inks, e.g. degree of shear thinning, ensures smooth and consistent extrusion while improving the shape fidelity of printed structures after deposition [17]. Lack of *in situ* curing in conventional DW limits the height of printed structures, especially if the print materials have a low working viscosity. Further, conventional DW methodologies typically recommend a post-curing step for thermoset inks after printing the entire 2D or 3D object to enhance mechanical performance.

We present a novel UV-assisted direct write (UADW) technique that combines extrusion-based direct write (DW) and *in situ* layer-by-layer UV curing to fabricate polymer-bonded magnets at room temperature. UV curing at each layer gives enough intermediate strength to allow the printed magnet to support itself during printing, while a final low-temperature post-curing step provides saturated curing and evaporation of any residual resin. The technique can print smooth-surfaced 3D objects with a layer-thickness resolution as high as 200 μm. To date, UV-assisted DW applications include 2D or single-trace 3D micro-coil printing [18], but no multi-layer 3D structures.

We created custom magnetic DW inks by mixing NdFeB powder with a UV-curable polymer binder. The DW process operates at room temperature, compared to around 300 °C for the FDM process [5]. A syringe extrudes the material, minimizing waste, especially as compared with the vat photopolymerization process. This low-temperature printing technique can readily integrate *in situ* with other AM processes—inkjet printing, aerosol jet printing, and pick-and-place process—to create 3D multi-functional electromagnetic objects. We present rheological optimization of custom-made inks and characterize UV curing efficiency as a function of particle loading to better understand printing constraints. Specifically, we investigate green and post-cured mechanical properties of printed dumbbell-shaped coupons. Further, we examine the dependence of magnetic properties on sample preparation factors, including material loading, layer thickness, and UV wavelength.

## 2. Experimental procedures

### 2.1. Materials

This study used resin-coated MQP-11-9 isotropic NdFeB magnetic powder feedstock from Magnequench. The original particles are spherical with an average diameter of 45 μm. We sieved powders with 25-μm mesh to reduce the average particle size. The raw powders have a specific gravity of 7.4 g/cm<sup>3</sup> and an apparent density of 3.7 g/cm<sup>3</sup>. The manufacturer reports an intrinsic coercivity ( $H_{ci}$ ) of 8.4–9.4 kOe and a residual induction ( $B_r$ ) of 7.3–7.6 kG. We used a Microtrac S3500 series particle size analyzer with tri-laser technology to determine the particle size distribution of the sieved powder and conducted dry measurements in triplicate using air as the medium to convey the sample to the measuring cell.

We selected Formlabs® grey photopolymer resin binder as the carrier for the NdFeB powder as it provides the highest NdFeB loading while maintaining sufficiently low viscosity for printing. Composed of methacrylate oligomers and monomers, the resin has a specific gravity of 1.1 g/cm<sup>3</sup>. According to Zguris [19], a UV curving wavelength of 405 nm would yield the best mechanical strength for the neat binder.

### 2.2. Direct-write printing

For the UV-assisted direct write (UADW) process, we employed nScript tabletop series micro-dispensing equipment. This pneumatically-driven dispensing system applies a continuous flow of ink through a nozzle. A shaft valve integrated into the dispensing assembly regulates the flow onto a 150 × 150 mm (L × W) substrate plate of flexible transparent polypropylene (Staples clear heavyweight sheet protector). Built into the machine is a UV lens with 405 nm or 365 nm wavelengths and an adjustable focal length. The penetration depth of UV into the photopolymer binder decreases as a function of increasing NdFeB particle loading. We can therefore maintain the as-printed layer thickness at 200 μm to ensure maximum curing.

During printing (Fig. 1), the system deposits the first layer onto a transparent substrate moving at a printing speed of 1 mm/s. Next, the UV light source irradiates the printed pattern at a moving speed of 2 mm/s following the same printing path. The distance between the UV lens and the printed structure remains at the optimal focal length of 50 mm. Each layer undergoes printing and curing before the deposition of the next layer. After printing and curing the entire structure, we invert the component and irradiate UV through the underside of the transparent substrate to further cure the bottom of the printed part. Mechanical removal from the substrate enables a freestanding product. We post-cured some as-printed samples (“green parts”) under a UVP B-100A high density multiple wavelength UV lamp; then heated them at 60 °C (Binder FED 115 oven) for 1 h to enhance curing and improve mechanical properties. We measured sample dimensions and weight to calculate the density of the printed products.

### 2.3. Rheological and mechanical experiments

We performed ink rheology experiments on DW inks containing 75, 80, 85, and 90 wt% of NdFeB powder. As a control, we also measured the rheology of the neat binder (i.e., 0 wt% NdFeB). An AR-G2 rheometer (TA Instruments) measured steady shear viscosities. We used a parallel plate fixture (diameter: 40 mm) with a gap of 600 μm and measured viscosities from high shear rate (100 s<sup>-1</sup>) to low shear rate (0.01 s<sup>-1</sup>) at a constant temperature of 25 °C.

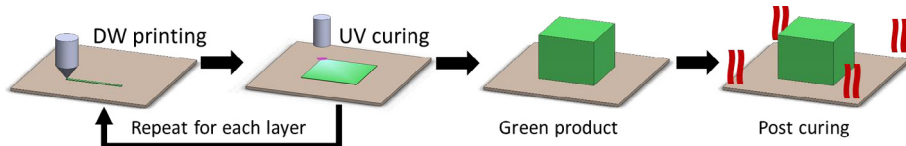


**Fig. 1.** Schematic diagram of the UV-assisted direct write (UADW) process for printing a cubic-shaped magnet.

The UADW process produced dumbbell-shaped test coupons with 5 layers and a nominal thickness of 1 mm. An Instron (Model 1011) mechanical analyzer characterized the mechanical properties, namely tensile strength and Young's modulus, of as-printed “green” samples. We tested coupons at different powder loadings (75, 80, 85, and 90 wt%), measuring and comparing the mechanical properties before and after secondary UV and heat curing for the highest loading of 90 wt%. Our system printed test coupons along the longer axis, i.e. tensile test direction. The manufacturer's data-sheet provided mechanical properties of post-cured neat binder [20]. To investigate the microstructure of the cured products and the mechanical failure mechanism, a HITACHI 3400S Scanning Electron Microscope (SEM) operated at an accelerating voltage of 10 kV was used.

#### 2.4. Magnetic properties measurements

We first pulse magnetized each sample with coil strength greater than 55 kOe to saturation and measured them in a Helmholz Coil along the sample height z-axis. We used a KJS Associates model HG-700 computer-automated magnetic hysteresigraph system to perform hysteresis loop measurements. Testing complies with ASTM A977/A977M-01, “Standard Test Method for Magnetic Properties of High Coercivity Permanent Magnet Materials Using Hysteresographs”.

### 3. Experimental results and discussions

#### 3.1. Particle size and ink rheology

**Fig. 2** shows the SEM image and the particle distribution of the sieved powder. The particles are largely spherical in shape and have an average diameter of 20.8  $\mu\text{m}$  with a standard deviation of 5.8  $\mu\text{m}$ . Morissette et al. [21] studied the optimal ink rheology for extrusion-based DW printing and concluded the nozzle size must be at least 10 times larger than the powder particle size to allow smooth printing without clogging. For this reason, we chose a gauge #25 stainless steel dispensing tip with a 250- $\mu\text{m}$  inner diameter.

**Fig. 3a** shows the steady shear rheology data for the neat binder and NdFeB dispersions with different powder loadings (0, 75, 80, 85 and 90 wt%). Within the range of shear rates studied, the neat

binder behaved essentially as a Newtonian fluid with a constant shear viscosity of ca. 0.9 Pa·s. Inclusion of NdFeB powder increased the dispersion viscosity, especially at lower shear rates, leading to shear thinning behavior (i.e., viscosity decreases as a function of increasing shear rate). The degree of shear thinning increases with increasing powder loading. Shear thinning is generally desirable for extrusion-based 3D printing: the ink experiences a higher shear rate and consequently sufficiently low viscosity for extrusion, but upon deposition, shear rate decreases such that a sufficiently high viscosity minimizes further fluid spread and improves shape fidelity. Based on this argument, Lewis [14] suggests the optimal apparent shear viscosity for DW printing as  $10^3$ – $10^4$  Pa·s at  $1\text{ s}^{-1}$ . In this study, the ink containing 90 wt% powder has an apparent shear viscosity of 500 Pa·s at  $1\text{ s}^{-1}$ , implying the ink may spread slightly after deposition. **Fig. 3b** characterizes the surface topography of a  $0.7 \times 0.5$  mm sample area of the top face of a cubic-shaped printed magnet. The sample area showed an arithmetic mean roughness ( $R_a$ ) of 0.923  $\mu\text{m}$  and a ten-point height ( $R_z$ ) of 44.21  $\mu\text{m}$  indicating a smooth surface finish. **Fig. 3c** shows coupons printed with 90 wt% powder loading.

#### 3.2. Mechanical properties

Literature indicates the maximum volume fraction of similar sized spherical particles in a confined volume with random close packing is 64% [22]. Experimentally the highest solid loading of a printable suspension achieved during mixing was 60% by volume, or 91% by weight. At extreme solid loading, particles could hinder cross-linking of the binder due to UV absorption and scattering, reducing the mechanical strengths of the printed parts. We employed post UV curing and heat treatment to enhance the mechanical strength of the as-printed products with 90 wt% NdFeB loading (**Fig. 4a**). Post-curing improved ultimate tensile strength from 2.43 MPa to 10.4 MPa, and Young's modulus from 577 MPa to 5.2 GPa, showing mechanical performance comparable to injection molding magnets and improvement over reported FDM printed samples [8]. Elongation at failure dropped from 1.7% to 0.6%, implying stronger but less ductile properties of the printed material. **Table 1** compares the mechanical properties of UADW coupons before and after post-curing against those prepared by BAAM as reported by Li [8]. After post-curing, UADW samples showed higher tensile strength and Young's modulus with slightly lower NdFeB powder loading.

**Fig. 4b** shows a typical fractured surface of the printed magnet after tensile tests. The figure shows magnetic particles removed from the adjacent layer during tensile testing, indicating debonding between NdFeB particles and cured binder as the primary cause of failure. Ferraris et al. report a similar failure mechanism for injection-molded and FDM-printed NdFeB magnets [8].

#### 3.3. Printed magnet characterization

**Fig. 5** presents some successfully printed magnets with arbitrary shapes and the top views of a cubic- and a ring-shaped printed magnet. One drawback of FDM and injection-molded magnets is the high porosity of their products due to filament geometries or air bubbles [5]. Measured density of FDM and

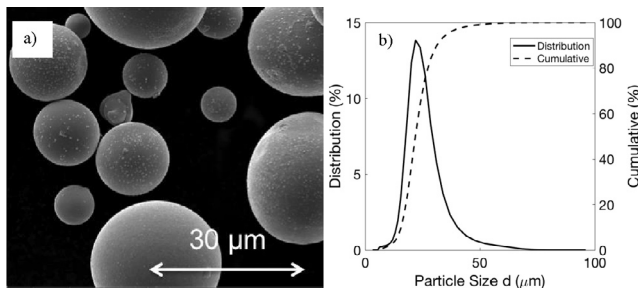


**Fig. 2.** a) Scanning Electron Micrograph (SEM) of as-received NdFeB powder.  
b) Particle diameter distribution of sieved NdFeB powder.

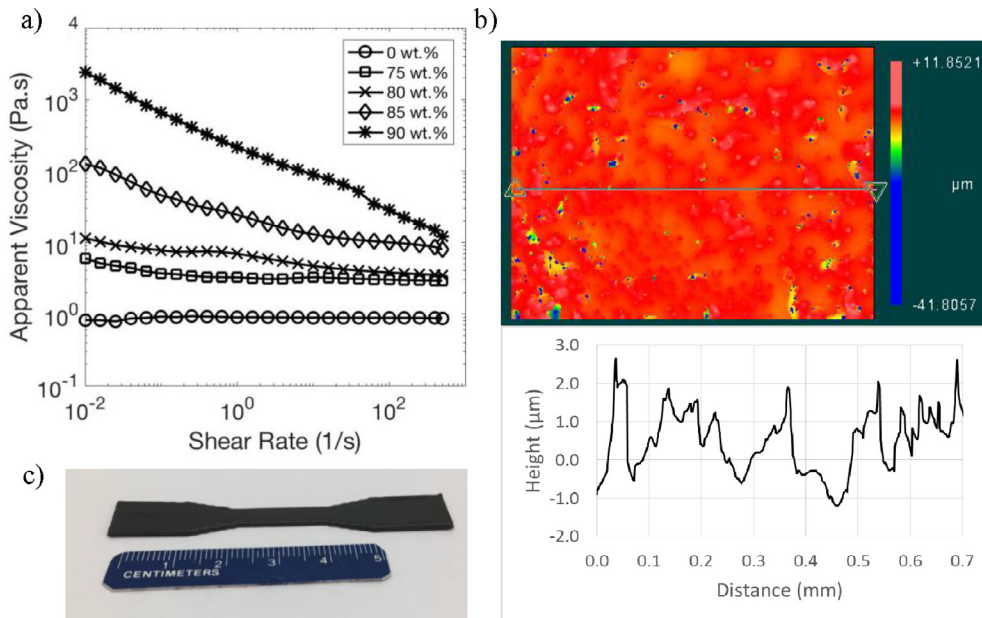


**Fig. 3.** a) Steady shear tests for NdFeB ink at different solid weight loadings. Temperature: 25 °C. b) White light interferometry surface profile of a 0.7 \* 0.5 mm sample area of the top face of a UADW cubic-shaped magnet. The line graph shows a 1D height sample along the x-axis, sampled from the horizontal line in the 2D image. c) A UADW dumbbell-shaped coupon with 90 wt% NdFeB loading.

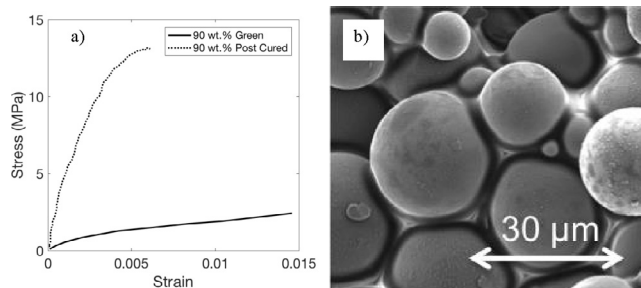


**Fig. 4.** a) Stress-strain curves of 90 wt% NdFeB coupon before and after post-curing, showing the effect of post-curing on mechanical properties. b) SEM image of fractured surface of a 90 wt% NdFeB post-cured coupon after tensile testing.

injection-molded magnets can be 10–20% lower than the theoretical density calculated from the starting nominal composition. Geometrically, voids between deposited filaments are characteristic of the FDM process. Extrusion-based DW uses a similar deposition mechanism, but the viscosity prior to in situ UV curing is comparatively lower. Surface tension can therefore drive fusion between deposited inks, minimizing or removing any voids between them. Experimentally, at 46% nominal volume fraction, the density of printed magnets measured 4.00 g/cm<sup>3</sup>, which closely matches the expected theoretical density of 3.99 g/cm<sup>3</sup> (assuming linear combination of input material densities and no voids). As the nominal volume fraction increased to 60%, however, the average density of the printed magnet sample increased to 4.23 g/cm<sup>3</sup> (based on three measurements), 10% lower than the expected theoretical density of 4.69 g/cm<sup>3</sup>. The difference is due to difficulty in dispersing the particles homogeneously as particle loading approaches the theoretical limit.

Theoretical density of 4.69 g/cm<sup>3</sup>. The difference is due to difficulty in dispersing the particles homogeneously as particle loading approaches the theoretical limit.

### 3.4. Magnetic properties

**Fig. 6a** shows the full hysteresis loop of post-cured magnets with three different volumetric concentrations calculated based on mixing component fractions. Remanence and intrinsic coercivity are key attributes of a magnet [10]. Remanence refers to the magnetization left behind in a ferromagnetic material after removing an external magnetic field, and intrinsic coercivity is the strength of the magnetic field necessary to reduce the magnetic polarization (strength of magnetization) to zero. In general, the higher the remanence value and the higher the intrinsic coercivity values, the stronger the magnet performance.

The 90 wt% NdFeB samples exhibited a remanence of 3.80 kGauss (52% of raw powder value) and intrinsic coercivity of 9.50 kOe. All three printed samples have similar intrinsic coercivities close to the raw powder value of 8.4–9.4 kOe; however, as the nominal volume fraction increased from 48% to 60%, remanence improved only 7% as shown in **Fig. 6a**. Therefore, it is more appropriate to back calculate the material composition from the final sample density, based on the known densities of raw powder and binder. **Fig. 6b** gives the relative remanence ( $B_r$ ) as a function of calculated volume fraction based on ten printed magnets with different densities. The trend is relatively linear with a coefficient of determination of 0.810 and indicates no significant energy loss during the magnetization process. It is worth noting that at the

**Table 1**

Comparison of mechanical properties of UV-assisted DW magnets (before and after post-curing with standard deviation based on 3 test coupons) against magnets prepared by the BAAM method [8].

Sample	Solid loading (by volume)	Tensile Strength [MPa]	Young's modulus [MPa]	Elongation at Failure
UADW (Green)	57%	2.43 ± 0.64	577 ± 123	1.7% ± 0.4%
UADW (Post-Cured)	57%	10.40 ± 2.46	5200 ± 1080	0.6% ± 0.2%
BAAM	60%	6.60	4290	4.1%

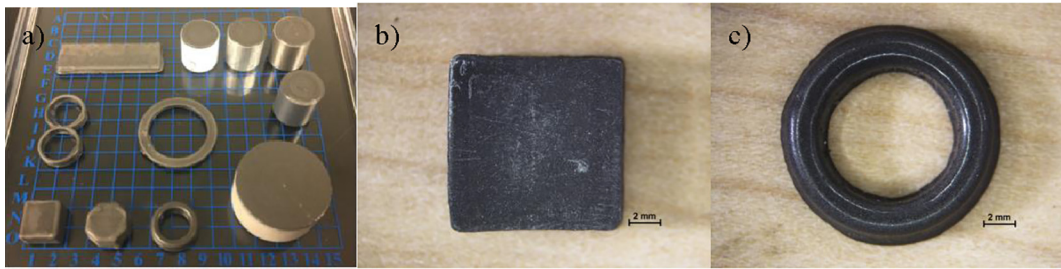


**Fig. 5.** a) Examples of UADW magnets with arbitrary shapes. b) Top view of a cubic-shaped magnet. c) Top view of a ring-shaped magnet.

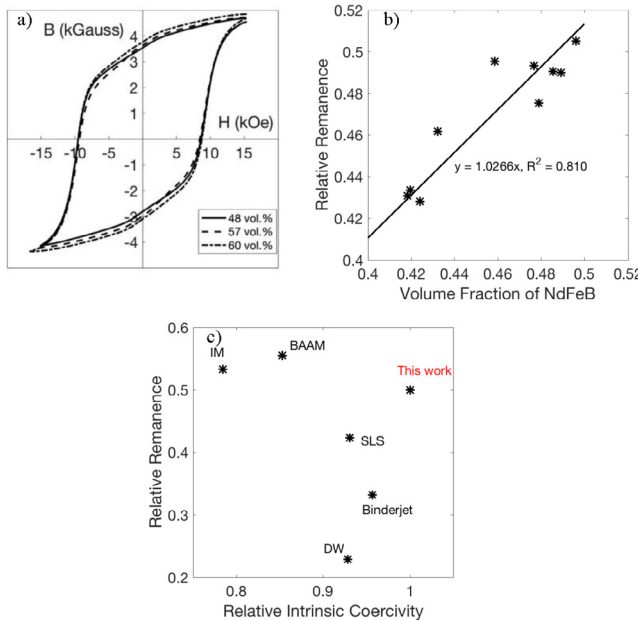


**Fig. 6.** a) Hysteresis loops of printed magnet samples with three nominal volume fractions. b) Relative remanence as a function of NdFeB loading. Relative remanence or intrinsic coercivity = sample remanence or intrinsic coercivity/raw powder remanence or intrinsic coercivity. c) Comparison of performance for magnets prepared by different methods, namely, UADW (this work), injection molding (IM) [8], big area additive manufacturing (BAAM) [8], selective laser sintering (SLS) [1], binder-jet [9], and direct write (DW) [10]. The higher the remanence value and the higher the intrinsic coercivity value, the better the magnet performance.

same powder loading, the final energy product of the magnets is an intrinsic property of the starting magnetic powder; thus, the performance of the printed magnets could be improved through the

use of NdFeB powders with stronger magnetic properties. The difference in raw powder also means when comparing magnet AM techniques, it is more reasonable to compare performance as a fraction of their raw powder properties (relative remanence or intrinsic coercivity = sample remanence or intrinsic coercivity/raw powder remanence or intrinsic coercivity). **Fig. 6c** compares the magnetic performance, both in terms of relative remanence and relative intrinsic coercivity, of magnets prepared by different 3D printing methods. Our UADW technique combines highest product intrinsic coercivity with one of the highest magnetic remanence values.

When using photopolymers as binder material, the percentage of curing affects product performance. Magnetic particles within a partially cured polymer matrix will have higher mobility and may become demagnetized when exposed to an opposite magnetic field, leading to a lower intrinsic coercivity. Due to different mechanisms between photo- and thermal curing, the degree of cure cannot be quantified simply based on the heat of reactions from differential scanning calorimetry. For magnets, however, intrinsic coercivity could indicate how well the sample is cured. **Fig. 7a** presents the second quadrant B-H curves for 85 wt% NdFeB magnets cured with two different UV wavelengths and printed at different layer thicknesses. The reported magnetic properties are for a cubic magnet with a dimension of  $10 \times 10 \times 6.2$  mm (length  $\times$  width  $\times$  height). While insufficient curing caused around a 13% remanence drop from 3.70 kG to 3.24 kG, poorly cured samples possess only 28% of the intrinsic coercivity of raw magnetic powder, and around 50% of the energy product of better-cured samples. Post-cured samples printed with a 200- $\mu\text{m}$  layer thickness and cured with a 405-nm wavelength had the same intrinsic coercivity as the raw magnetic powder, indicating sufficient curing. From observations, longer UV wavelength allows for deeper penetration into the opaque magnetic layers; alternatively, minimizing layer thickness would also help crosslinking of the photopolymer and interlocking

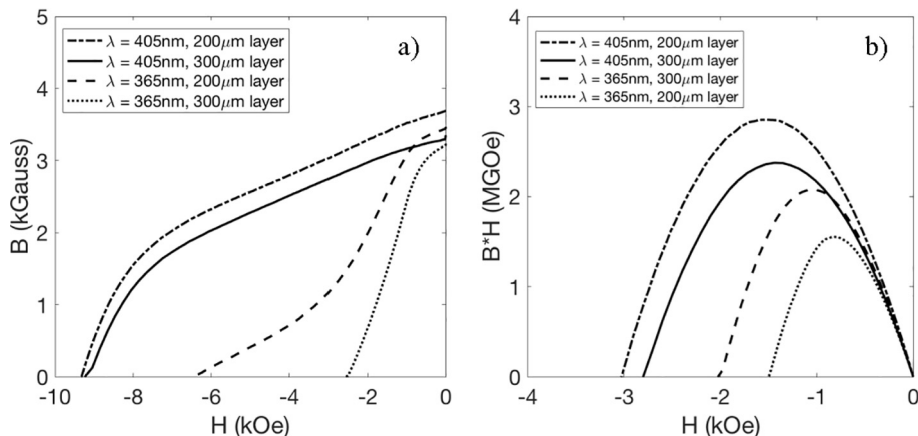


**Fig. 7.** a) Second quadrant hysteresis curve of printed post-cured NdFeB magnets with different UV wavelengths and layer thicknesses. b) Energy product of printed post-cured NdFeB magnets with different UV wavelengths and layer thicknesses.

of magnetic particles. Fig. 7a suggests that to increase the degree of cure, changing the UV wavelength is more effective than reducing layer thickness.

For both FDM and injection-molded magnets, the intrinsic coercivity of the final product deteriorated relative to that of the raw material. Depending on the polymer filament or the binder material, melting the feed mixture often requires temperatures of 300 °C or higher. Higher process temperatures and/or longer residence times could cause grain growth or microstructure changes and have been proposed as possible explanations for the deterioration in magnet performance [8]. In contrast, UADW calls for printing and curing *in situ* at room temperature. Post-curing at 60 °C can increase the degree of cure, but the temperature is still considerably lower than those typically used for FDM or injection molding and may explain the better performance of the UADW magnets.

#### 4. Conclusions

Additive manufacturing of polymer-bonded magnets with spherical isotropic powders shows great potential to reduce cost and create intricate geometries with arbitrary shapes. Current methods for 3D printing magnets, such as fused deposition modeling (FDM), typically involve high-temperature processing which compromises the intrinsic coercivity and energy product of the printed magnets. This paper presents a novel UV-assisted direct write (UADW) method that combines extrusion-based DW with *in situ* layer-by-layer UV curing to fabricate polymer-bonded magnets at room temperature. The process requires minimal post heat treatment and preserves the magnetic properties of the raw powder in the printed product. We characterized the rheology of custom-created DW inks containing an NdFeB loading of up to 91 wt%, or 60% by volume. We explored the print-layer thickness and UV-curing wavelength to maximize the degree of curing, which is critical to locking the NdFeB particles in place and preventing demagnetization. The mechanical properties of UADW magnets include a tensile strength of 10.4 MPa and a Young's modulus of 5.2 GPa after post-curing, showing improvements over magnets with similar particle loading produced by the Big Area Additive Manufacturing (BAAM) method. Further, the intrinsic coercivity and remanence of UADW magnets normalized by the raw powder values outperform values reported in the literature for magnets prepared from other additive manufacturing methods, including FDM, selective laser sintering (SLS), binder-jet, and direct write (DW). The magnets reported in this paper possess the highest intrinsic coercivity with one of the highest magnetic remanence values, characteristics attributable to the low processing temperature, which preserves the intrinsic coercivity of the raw powder. For future work, magnet performance may be further improved by optimal selection of raw powder, binder, and print conditions.

#### Acknowledgement

The team acknowledges financial support from United Technologies Research Center (UTRC), Connecticut Space Grant Consortium, and Anton Paar Research Fellowship.

#### Appendix A. Supplementary data

Supplementary data associated with this article can be found, in the online version, at <https://doi.org/10.1016/j.jmmm.2018.03.073>.

#### References

- [1] (a) J. Faiz, H. Nejadi-Koti, Z. Valipour, *IET Electric Power Appl.* 11 (2017) 142; (b) H. Shokrollahi, *J. Magn. Magn. Mater.* 426 (2017) 74.
- [2] K. Elian, & H. Theuss. Integration of Polymer Bonded Magnets into Magnetic Sensors (2014).
- [3] L. Ferraris, F. Franchini, & E. Poskovic. Hybrid magnetic composite (HMC) materials for sensor applications, in: SAS 2016 – Sensors Applications Symposium, Proceedings (2016) 134–139.
- [4] D. Zhang, J. Xiao, Y. Qiu, J. Yang, & Q. Guo. Initiator-Integrated 3-D Printing of Magnetic Object for Remote Controlling Application (2017) 53(5).
- [5] S. Kim, F. Qiu, S. Kim, A. Ghanbari, C. Moon, L. Zhang H. Choi, Fabrication and characterization of magnetic microrobots for three-dimensional cell culture and targeted transportation, *Adv. Mater.* 25 (41) (2013) 5863–5868.
- [6] C. Huber, C. Abert, F. Bruckner, M. Groeneweld, O. Muthsam, S. Schuschnigg D. Suess, 3D print of polymer bonded rare-earth magnets, and 3D magnetic field scanning with an end-user 3D printer, *Appl. Physics Lett.* 109 (16) (2016).
- [7] A.S. El-gizawy, S. Corl, & B. Graybill. (n.d.). Process-induced Properties of FDM Products.
- [8] (a) L. Li, A. Tirado, I.C. Nlebedim, O. Rios, B. Post, V. Kunc M.P. Paranthaman, Big area additive manufacturing of high performance bonded NdFeB magnets, *Sci. Rep.* 6 (1) (2016) 36212; (b) L. Li, B. Post, V. Kunc, A.M. Elliott, M.P. Paranthaman, Additive manufacturing of near-net-shape bonded magnets: prospects and challenges, *Scri. Mater.* 135 (2016) 100–104.
- [9] M.P. Paranthaman, C.S. Shafer, A.M. Elliott, D.H. Siddel, M.A. McGuire, R.M. Springfield J. Ormerod, Binder jetting: a novel NdFeB bonded magnet fabrication process, *JOM* 68 (7) (2016) 1978–1982.
- [10] B.G. Compton, J.W. Kemp, T.V. Novikov, R.C. Pack, C.I. Nlebedim, C.E. Duty M.P. Paranthaman, Direct-write 3D printing of NdFeB bonded magnets, *Mater. Manuf. Processes* (2016) 1–5.
- [11] L. Donaldson, 3D printed magnets with little waste, *Mater. Today* 20 (2) (2017) 54.
- [12] J.W. Halloran, Ceramic stereolithography: additive manufacturing for ceramics by photopolymerization, *Annu. Rev. Mater. Res.* 46 (2016) 19–40.
- [13] R.J. Mondschein, A. Kanitkar, C.B. Williams, S.S. Verbridge, T.E. Long, Polymer structure-property requirements for stereolithographic 3D printing of soft tissue engineering scaffolds, *Biomaterials* 140 (2017) 170–188, <https://doi.org/10.1016/j.biomaterials.2017.06.005>.
- [14] (a) J.A. Lewis, Direct ink writing of 3D functional materials, *Adv. Funct. Mater.* 16 (17) (2006) 2193–2204; (b) A. Piqué, in: *Direct-write Technologies for Rapid Prototyping Sensors, Electronics, and Integrated Power Sources*, Academic Press, 2002, pp. 1–551; (c) J.A. Lewis, G.M. Gratson, Direct writing in three dimensions, *Mater. Today* 7 (7) (2004) 32–39.
- [15] (a) Method for manufacturing layered electronic devices. S. Culp, S. Dardona, & W. Schmidt – US Patent 9,832,875 (2017). (b) Method for fabricating printed electronics. S. Dardona, W.R. Schmidt, & S.R. Culp – US Patent App. 14/333,837 (2014). (c) S. Dardona, J. Hoey, Y. She, & W.R. Schmidt, Direct write of copper-graphene composite using micro-cold spray. *AIP Advances* (2016) 6(8); (d) S. Dardona, A. Shen, Ç. Tokgöz, *IEEE Sensor. J.* 18 (8) (2018) 3461–3466.
- [16] (a) R.D. Farahani, H. Dalir, V. Le Borgne, L.A. Gautier, M.A. El Khakani, M. Lévesque, & D. Therriault, Direct-write fabrication of freestanding nanocomposite strain sensors. *Nanotechnology* (2012) 23(8), 85502. (b) Y. Zhang, C. Liu, & D. Whalley, Direct-write techniques for maskless production of microelectronics: A review of current state-of-the-art technologies. 2009 in: *International Conference on Electronic Packaging Technology and High Density Packaging, ICEPT-HDP 2009* (2009) 497–503.
- [17] B. King, S.L. Morissette, H. Denham, J. Cesario, & D. Dimos, (n.d.). Influence of rheology on deposition behavior of ceramic pastes in *illJill'Jil*, 391–398.
- [18] (a) Rouhollah Dermanaki Farahani, Direct-write fabrication of freestanding nanocomposite strain sensors, *Nanotechnology* 23 (8) (2012) 1–9; (b) L.L. Lebel, B. Aissa, M.A. El Khakani, D. Therriault, Ultraviolet-assisted direct-write fabrication of carbon nanotube/polymer nanocomposite microcoils, *Adv. Mater.* 22 (5) (2010) 592–596.
- [19] Z. Zguriš, How Mechanical Properties of Stereolithography 3D Prints are Affected by UV Curing. Formlabs White Paper. (2016). Retrieved from <https://formlabs.com/media/upload/How-Mechanical-Properties-of-SLA-3D-Prints-Are-Affected-by-UV-Curing.pdf>.
- [20] Formlabs Inc. Clear Photopolymer Resin for Form 1+ and Form 2 - Material properties. [Www.Formlabs.Com](http://www.formlabs.com), 3–5. (2016) Retrieved from <https://formlabs.com/media/upload/Clear-DataSheet.pdf>.
- [21] S.L. Morissette, J.A. Lewis, P.G. Clem, J. Cesario, D.B. Dimos, Direct-write fabrication of Pb(Nb, Zr, Ti)O<sub>3</sub> devices: influence of paste rheology on print morphology and component properties, *J. Am. Ceram. Soc.* 84 (11) (2001) 2462–2468.
- [22] (a) R.S. Farr, Random close packing fractions of lognormal distributions of hard spheres, *Powder Technol.* 245 (2013) 28–34; (b) Y. Wu, Z. Fan, Y. Lu, Bulk and interior packing densities of random close packing of hard spheres, *J. Mater. Sci.* 38 (9) (2003) 2019–2025.